

# Appearance and Disappearance of Dendritic and Chiral Patterns in Domains of Langmuir Monolayers Observed with Brewster Angle Microscopy

Frank Hoffmann,<sup>†</sup> Keith J. Stine,<sup>‡</sup> and Heinrich Hühnerfuss<sup>\*,†</sup>

*Institute of Organic Chemistry, University of Hamburg, Martin-Luther-King-Platz 6, 20146 Hamburg, Germany, and Department of Chemistry & Biochemistry and Center for Molecular Electronics, University of Missouri—St. Louis, 8001 Natural Bridge Road, St. Louis, Missouri 63121*

*Received: December 31, 2003; In Final Form: September 1, 2004*

Investigations on the aggregation behavior and morphology of Langmuir films of enantiomeric (L) and racemic (DL) *N*-acyl amino acids on pure aqueous as well as metal cation containing subphases were carried out at the mesoscale level with the help of Brewster angle microscopy (BAM). In the case of *N*-hexadecanoyl alanine on a pure aqueous subphase at 298 K the L-enantiomer forms crystal platelets, while the irregular fractal-like shape of the domains of the racemic mixture can be explained by a diffusion limited aggregation (DLA) growth mechanism. At 303 K the L-enantiomer shows a dendritic growth pattern, which leads to explicitly chiral domain shapes that correspond with the chirality of the film-forming molecules and for which hydrogen bridges as directed attractive forces are assumed to be responsible. The compression of the L-enantiomer on a zinc ion containing subphase is accompanied by a remarkable metamorphosis of the condensed structure. Starting from torus-like domains they were at first converted into strongly wound S-shaped domains, finally turning into a seahorse-like appearance. The origin of these chiral shapes can be explained on the basis of an electrostatic growth model. The enantiomer of *N*-hexadecanoyl alanine methyl ester shows three different asymmetric dendritic growth patterns. The domains of the racemic mixture are dendritic too, but in contrast they are symmetric and have a notably low branching density. On a pure aqueous subphase the L-enantiomer of *N*-octadecanoyl valine exhibits dendritic growth as well, but the overall outer shape of the domains is not explicitly chiral.

## Introduction

Chirality and enantioselective interactions are omnipresent in chemical and biological systems, playing a key role in the assembly of supramolecular structures and recognition events. Common examples are enzymes and their constituent amino acids, carbohydrates, DNA and its constituent nucleotides, and membranes with their asymmetric integral membrane proteins and phospholipids. The question of how and why chiral molecules involved in life processes only occur in one and the same enantiomeric form, known as the phenomenon of the homochirality of life, has challenged scientists for almost 150 years. Many possible theoretical explanations have been put forward (see, for instance, ref 1 and literature cited therein), including the influx of extraterrestrial material<sup>2</sup> and the effect of cosmic chirality,<sup>3</sup> none of which is fully satisfactory. However, in the past two decades a variety of experimental evidence has been reported, showing that (i) an achiral or racemic system can spontaneously evolve into an (almost) monochiral state, particularly during crystallization,<sup>4–7</sup> (ii) a small enantiomeric excess, produced by stochastic fluctuations, can be amplified in autocatalytic reactions,<sup>8–10</sup> even in monolayers as recently shown by Zepik et al.,<sup>11</sup> (iii) achiral molecules can form chiral phases and exhibit chiral symmetry breaking,<sup>12,13</sup> and (iv) mixtures of enantiomers can undergo chiral phase separation processes,<sup>14</sup> especially in monolayers.<sup>15–20</sup>

The latter case is, e.g., represented by Langmuir monolayers at the air/water interface. They are well suited to study chiral discrimination effects, as these effects are often very pronounced. Experimental approaches have mostly focused on comparing the characteristic surface parameters of the enantiomeric film with those of the racemic mixture.<sup>21</sup> Potential chiral discrimination tendencies can be concluded from different experimental techniques, such as  $\Pi/A$  isotherm measurements; from optical techniques, such as fluorescence and Brewster angle microscopy (BAM); from vibrational spectroscopy techniques, such as infrared reflection–absorption spectroscopy (IRRAS); and from lattice structural information based on grazing incidence X-ray diffraction (GIXD) studies. Accordingly, the discrimination effects can manifest themselves in various ways, comprising a large range of length scales, such as features of the isotherm, shapes and textures of the domains formed in the condensed phase, and differences in lattice structures.

In films where the constituent amphiphiles exhibit one stereogenic center, the chiral discrimination effect can be described either as homochiral discrimination, if the D:D or L:L attractive interaction is stronger, or as heterochiral discrimination, if the D:L interaction is stronger. Homochiral interactions are of particular interest, because they raise the possibility of partial or complete phase separation into domains of L- and D-enantiomers.

Over the past 10 years, monolayers of chiral amphiphiles with amino acid headgroups have attained great attention.<sup>22–44</sup> The amino acid, chain length, subphase composition, and temperature were varied, and the monolayers were studied with the help of different techniques. Recently, Mao et al.<sup>45</sup> carried out a lattice

\* Corresponding author. Phone: +49-40-42838-4240. Fax: +49-40-42838-2893. E-mail: huehnerfuss@chemie.uni-hamburg.de.

<sup>†</sup> University of Hamburg.

<sup>‡</sup> University of Missouri—St. Louis.

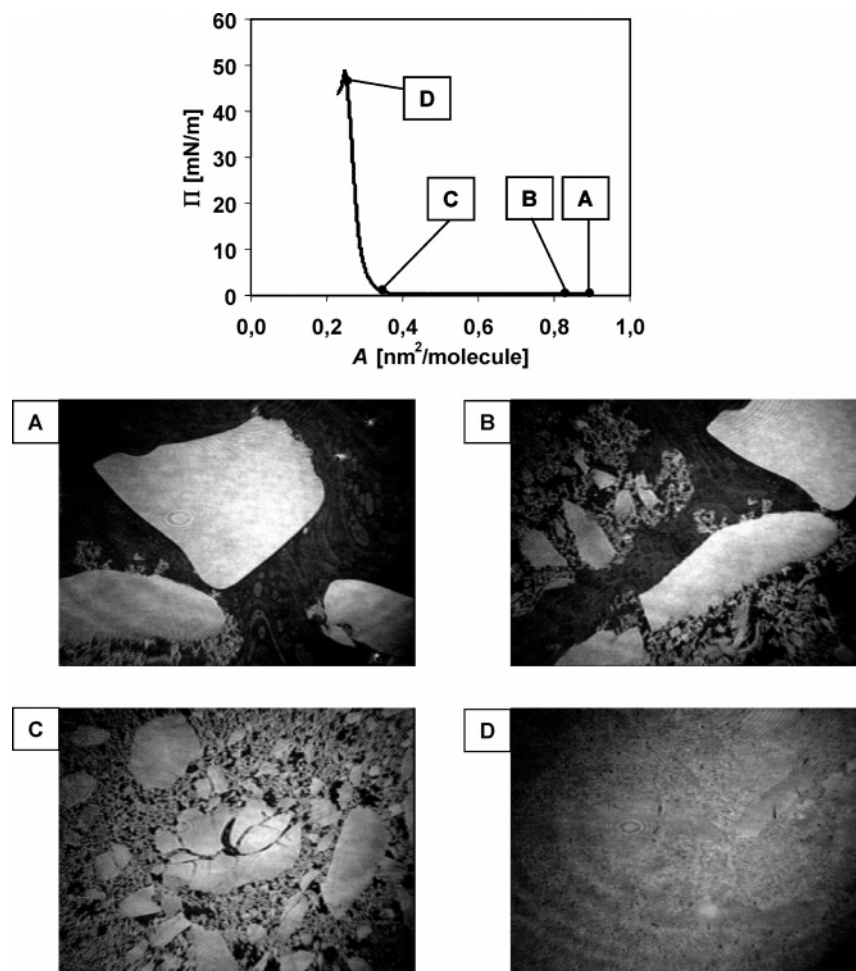


**Figure 1.**  $\Pi/A$  isotherm and corresponding BAM images (A–D) of *N*-hexadecanoyl L-alanine on a pure aqueous subphase (pH 2,  $T = 298$  K). The images were recorded at the points indicated on the  $\Pi/A$  plot. They represent an area of  $W \times H = 6 \times 4$  mm.

simulation (cellular automata calculation) of chiral discrimination effects in monolayers based on the theoretical “tripod model” introduced by Andelman.<sup>46,47</sup> They were able to reproduce the formation of segregated domains in racemic monolayers with homochiral interactions. Another theoretical approach was developed by Nandi and Vollhardt,<sup>48–50</sup> which is based on an effective pair potential (EPP) between the interacting chiral amphiphiles. Although some progress was achieved, in particular, with regard to the prediction of handedness of domains, a complete understanding of the mechanisms leading to the discriminating effects that emerge on the different length scales has yet to be developed.

In the present study enantiomeric and racemic monolayers of *N*-hexadecanoyl alanine, its methyl ester, and *N*-octadecanoyl valine on pure aqueous and metal ion containing subphases were investigated with the help of BAM. It can be regarded as a complementary work with the aim of filling the explanatory gap between the already attained thermodynamic ( $\Pi/A$  measurements) and spectroscopic data (IRRAS) of these systems, which revealed a few uncertainties and even contradictions.<sup>42</sup> Special emphasis is placed on the following questions: whether enantioselective phase separation processes can be detected, whether the molecular chirality is reflected in the mesoscaled supramolecular assemblies of the domains, and which parameters could be responsible for the specific domain textures observed. In the current study, it should be kept in mind that the domains observable in these experiments are often non-equilibrium growth forms. The objective of this study was not to investigate the transport properties of the monolayers in detail,

for instance the evolution of dendrites in terms of time or relaxation phenomena during domain shape transitions. The disposed equipment would not have been suitable for that purpose. Unlike the case of phospholipids or fatty acids which will form dendritic or fractal-like domains on high compression rates that can undergo shape transitions as they relax toward more compact equilibrium forms,<sup>51–53</sup> *N*-acyl amino acid surfactants are attracted to each other through comparatively strong directional forces mediated by hydrogen bonds. Their monolayer domains are not expected to relax as easily as those of phospholipids or fatty acids which lack comparatively strong forces. Fractal-like domains of myristic acid formed by rapid compression required tens of minutes to relax to circular forms at 299 K, with more rapid relaxation at lower temperatures due to increased line tension.<sup>51</sup> A relaxation time of at least 5 h was reported for chiral dendritic domains formed by L-DPP-(Me)E after rapid compression.<sup>52</sup> For fractal-like domains of DPPC formed under intermediate–high compression rates, no relaxation was observed on the time scales studied, while those of DMPE relaxed to the equilibrium shapes.<sup>53</sup> These examples may indicate how sensitive the domain relaxation kinetics depend on variations in molecular structure. For DMPE, a compression rate of  $0.002 \text{ nm}^2 \text{ molecule}^{-1} \text{ min}^{-1}$  resulted in equilibrium domain shapes. Instead of focusing on details of domain growth, the present study concentrates on the subject of how molecular and macroscopic chirality are related to each other. Furthermore, the BAM was used to check if chiral phase separation processes (demixing of the enantiomers) will occur

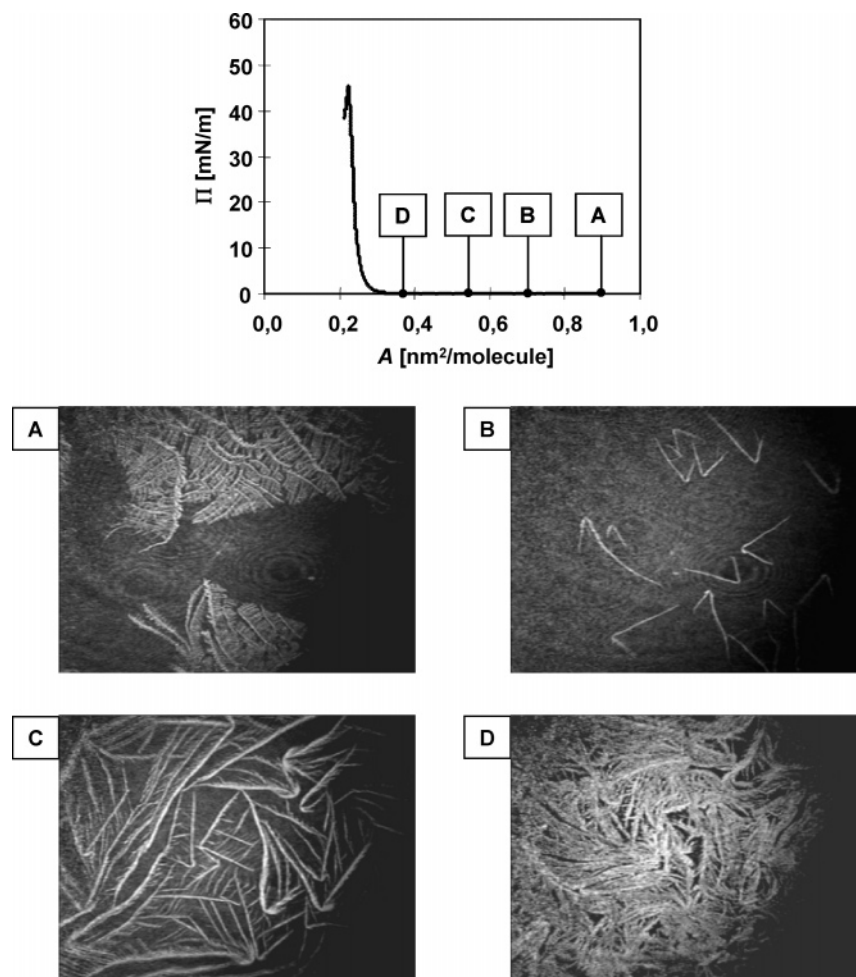


**Figure 2.**  $\Pi/A$  isotherm and corresponding BAM images (A–D) of *N*-hexadecanoyl L-alanine on a pure aqueous subphase (pH 2,  $T = 303$  K). The images were recorded at the points indicated on the  $\Pi/A$  plot. They represent an area of  $W \times H = 6 \times 4$  mm.

for cases in which homochirality is the preferential interaction as deduced from complementary earlier investigations.<sup>29,42</sup>

### Experimental Section

The water for the pure and metal ion containing subphases was deionized and purified (conductivity  $< 0.05 \mu\text{S}$ ) by a Seralpur Pro 90C apparatus (Seral, Ransbach, Germany). In order to ensure that the surfactants with free carboxylic acid groups are in an undissociated state, the pH value of the subphase was adjusted to 2 by adding an appropriate amount of hydrogen chloride (35%, analytical reagent grade; Merck, Darmstadt, Germany); in all other cases the pH value was in the range 5.7–6.0. The metal salt (calcium dichloride dihydrate  $\geq 99.9\%$ , zinc dichloride  $\geq 99.9\%$ ; Merck, Darmstadt, Germany) concentrations of the metal ion containing subphases were  $1.0 \times 10^{-3} \text{ mol L}^{-1}$ .

About 20 min after spreading of the surfactant solutions (solvent  $\text{CHCl}_3$ ; concentration  $1.4 \times 10^{-3} \text{ mol L}^{-1}$ ) the  $\Pi/A$  isotherms were recorded with the help of a Lauda FW-2 Langmuir film balance (Lauda-Königshofen, Germany) that was temperature controlled in the limits of  $\pm 0.1$  K. The compression rate was about  $0.006 \text{ nm}^2 \text{ molecule}^{-1} \text{ min}^{-1}$  and was the smallest possible. It should be stressed that the rate was similar to the one used for the IRRAS and Langmuir film balance investigations as should be the case for reasons of comparability.

The BAM (MiniBAM; Nanofilm Technologie GmbH, Göttingen, Germany) was mounted on a Langmuir film balance type A (Lauda-Königshofen, Germany). Both were stored in a

glovebox to avoid dust contamination and air turbulence. The BAM is equipped with a 688 nm laser (30 mW), the lateral resolution of the BAM is about  $20 \mu\text{m}$ , and the field of view is  $6 \times 4$  mm. By means of an integrated image correction the BAM supplied images with a very low geometric distortion. Because the BAM lacks an analyzer, reflectivity inversion tests could not be carried out. An integrated CCD camera supplied a video signal from which the images were captured with a video card (miroVIDEO D1, miro/Pinnacle Systems, USA). After the images were stored on a hard disk, they were optimized with regard to their brightness, hue, contrast, and sharpness with an image processing software package.

### Results and Discussion

***N*-Hexadecanoyl L-Alanine/ $\text{H}_2\text{O}$ .** The morphologies of the enantiomeric monolayer of *N*-hexadecanoyl L-alanine were investigated at two different temperatures (298 and 303 K). Although the  $\Pi/A$  isotherms were nearly identical, the morphological features exhibited remarkable differences. The  $\Pi/A$  isotherm recorded at 298 K and a series of BAM images taken during the compression are shown in Figure 1. Immediately after the spreading procedure, crystalline islands with sizes up to several millimeters are formed (image A). They coexist with and are surrounded by smaller tress-like structures. Large fractions of the BAM image areas in A and B appear dark, representing the gas phase in which the surface density is very low. This observation is expected for the coexistence of a condensed monolayer phase with the gas phase, and is consistent



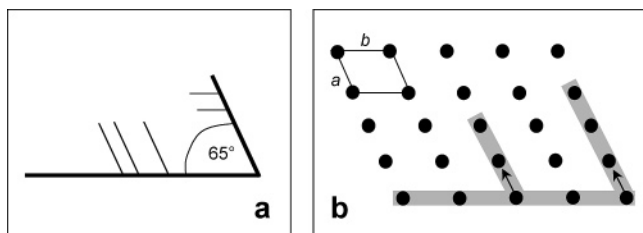


**Figure 3.** (a) Schematic geometric representation of the domains of *N*-hexadecanoyl L-alanine in the early stage of compression at  $T = 303$  K. (b) Proposed model of correlation between the crystal structure and the domain shape. The positions of the amphiphiles are indicated as filled circles; the gray lines represent the main growth directions. The arrows show the possible direction of the azimuthal tilt. In the top left corner the oblique subcell is drawn with the lattice vectors  $a$  and  $b$ .

with the  $\Pi/A$  isotherm in Figure 1 in which  $\Pi$  is near zero until rising at lower molecular areas with no evidence of formation of a liquid-expanded phase. In summary, a picture of an arctic pack-ice-like landscape is visible. With ongoing compression more condensed structures were formed and the big single crystalline islands were pushed together, without any appreciable increase in the surface pressure (image C). This observation is consistent with the expectation from the lever rule that the fraction of the surface covered by the condensed phase will increase as the monolayer is compressed along the low-pressure part of the  $\Pi/A$  isotherm. Some of the islands are fractured; therefore, it can be concluded that they are brittle in nature. Finally, the surface pressure steeply increases within a very small

compression range until an almost uniform coverage of the surface is achieved (image D). These morphologies are typical of monolayers with highly ordered solid-like phases observed at low temperatures where the  $\Pi/A$  isotherm does not exhibit a part that can be assigned to a liquid-expanded phase; see, for instance, refs 54 and 55. The islands appear immediately after the spreading procedure, and the size of the islands increases with increasing concentration of the spreading solution (data not shown), but not in the course of the compression. The observation that almost all of the solid-like domains appear just after the spreading procedure, with few if any new ones appearing later during the course of compression, is consistent with a strong tendency of the molecules to aggregate. The overall area fraction of solid-like domains should be consistent with the lever rule. However, we do not know the molecular area for the gas phase. The overall outer shape of the solid-like islands shows neither regular nor chiral characteristics, so the molecular chirality of the film forming amphiphiles is not reflected in their domain shapes.

At 303 K totally different morphologies were observed (Figure 2). During the spreading procedure extended curved dendritic domains were formed (image A). However, they disappeared within about 30 min. After compression, at  $\sim 0.7$  nm<sup>2</sup>/molecule condensed structures appeared again. In contrast to the former domains, they exhibit a hook-like shape (image B). A closer look reveals additional remarkable features: they are two-dimensionally chiral and all of them are of the same sort, i.e., the “sign” of their chirality is in all cases identical, and mirror images of these small hooks could not be observed.

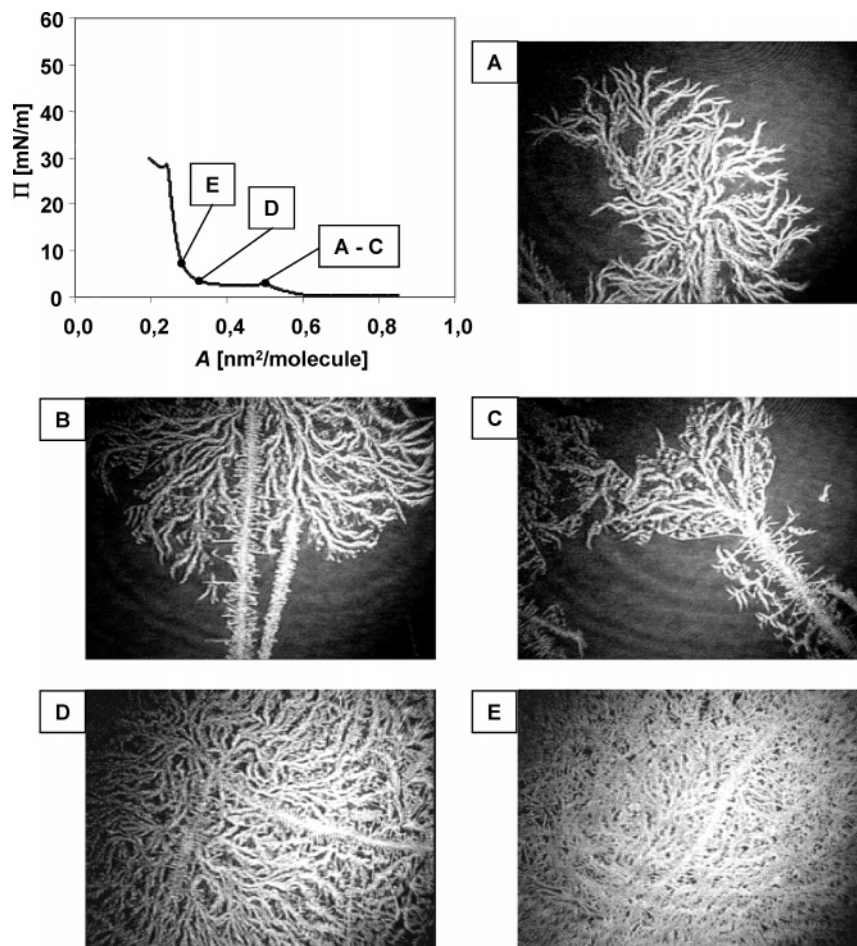


**Figure 4.**  $\Pi/A$  isotherm and corresponding BAM images (A–E) of *N*-hexadecanoyl DL-alanine on a pure aqueous subphase (pH 2,  $T = 298$  K). The images were recorded at the points indicated on the  $\Pi/A$  plot. They represent an area of  $W \times H = 6 \times 4$  mm.

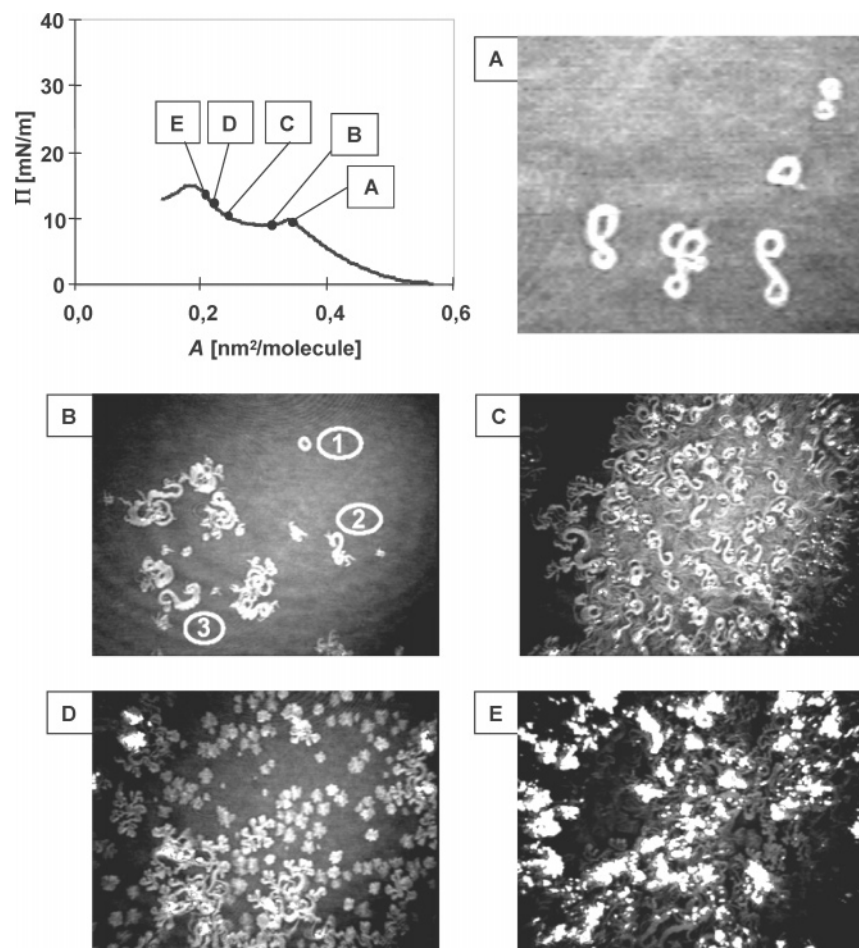


**Figure 5.**  $\Pi/A$  isotherm and corresponding BAM images (A–E) of *N*-hexadecanoyl L-alanine on a zinc cation containing subphase (pH 6,  $T = 298$  K). The images were recorded at the points indicated on the  $\Pi/A$  plot. They represent an area of  $W \times H = 6 \times 4$  mm (B–E) and  $2 \times 1.5$  mm (A), respectively. The numbers ①, ②, and ③ in image B are explained in the text.

Note that a mirror plane symmetry element, prevalent in three dimensions, is absent in the two-dimensional (2D) counterpart because, at the air/water interface, amphiphilic molecules are perforce oriented with their hydrocarbon chains emerging into the air. With progressive compression dendritic structures are developed, where the main strands of the hooks can be identified as the main growth directions, preferentially increasing in length, but only slightly in width, including the ramification of some additional shorter branches (image C). Finally, the dendritic structures become more and more dense (image D). At this temperature, the  $\Pi/A$  isotherm also indicates coexistence of a gas phase with a solid-like phase, and throughout this entire coexistence region, the surface pressure should remain constant and very low. Concerning the question of whether the hook-like domains are true monolayers or not, the area/molecule value where the surface pressure begins to rise is a hint that this is indeed the case; the value is consistent with the cross section of this class of amphiphiles ( $0.24 \text{ nm}^2/\text{molecule}$ ). Unfortunately, the MiniBAM is not equipped with an analyzer; therefore, a test of domain reflectivity inversion could not be carried out. Without an analyzer, intensity variations within domains associated with possible anisotropic molecular orientation are not observable. Parazak et al.<sup>29</sup> also observed dendritic domain structures in a fluorescence microscopic study of *N*-hexadecanoyl L-alanine at 308 K, but they failed to record images of the explicitly chiral hooks at the very early stage of the development/compression course.

Dendritic or fractal-like structures can be expected for all classes of systems where the growth is determined by the diffusion limited aggregation (DLA) mechanism, introduced by Witten and Sander in 1981.<sup>56,57</sup> For 2D systems such as monolayers, other approaches were developed to explain the evolution of these dendritic structures including the flow-controlled growth mechanism by Bruinsma et al.,<sup>58</sup> which is based on the Marangoni flow, and the two-dimensional diffusional growth mechanism by Brener et al.<sup>59</sup> The first mentioned approach leads to ramified structures of irregular (isotropic) fractal or dendritic shape, while the latter is in principle suitable to explain the occurrence of anisotropic shapes through the introduction of a parameter describing the strength of the surface tension anisotropy. In order to introduce anisotropy, the existence of a directional force between the interacting particles of the growing dendrites is necessary, which leads to preferential growth directions in contrast to cases where the dominating forces are isotropic, such as van der Waals interactions between simple fatty acid amphiphiles, which tend to form more compact domain shapes. Therefore, we assume that directed amide–amide H-bonds between the polar headgroups of the *N*-acyl amino acid amphiphiles are responsible for the evolution of these dendritic structures. Although it is in general not possible to predict the three-dimensional crystal structure by inspecting the isolated molecule, a few attempts were successful in those cases where H-bonds were involved.<sup>60</sup> However, it should be possible to correlate the macroscopic two-dimensional domain shapes

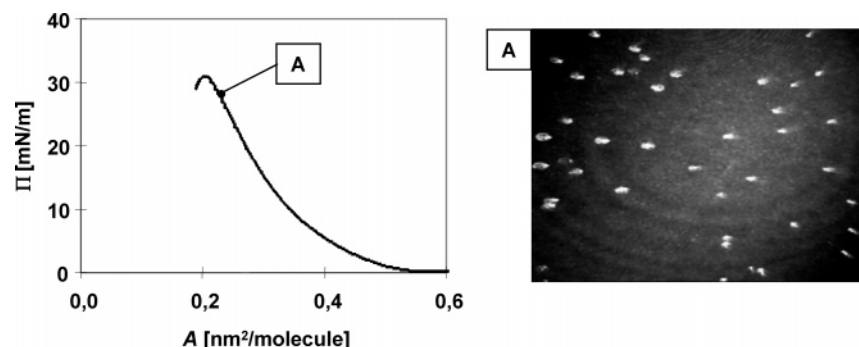


**Figure 6.**  $\Pi/A$  isotherm and one corresponding BAM image (A) of *N*-hexadecanoyl DL-alanine on a zinc cation containing subphase (pH 6,  $T = 298$  K). The image was recorded at the point indicated on the  $\Pi/A$  plot. It represents an area of  $W \times H = 6 \times 4$  mm.

with the underlying lattice more easily than in three-dimensional cases.<sup>61</sup> Furthermore, it is reasonable to assume that the highest positional long-range order is attained along the directed bond,<sup>62</sup> i.e., along the H-bond. According to this assumption and taking into account the geometric features of the dendritic domains (the main strands have an intersecting angle of about  $65^\circ$ ), an oblique subcell (this is the most common type of subcell for enantiomeric amphiphiles) is proposed as depicted in Figure 3. The hydrogen bonds are oriented along the shorter lattice vector *a* (the typical distance for an amide–amide H-bond is 0.49 nm), forming the shorter main strand of the hook and the smaller branches parallel to it, and the longer main strand is oriented along the lattice vector *b*. Without performing grazing incident X-ray diffraction (GIXD) measurements, it is not possible to determine the azimuthal angle orientation of the amphiphiles, but it is known that nearest-neighbor (NN) orientation is preferred in these early compression states. This would be the direction of the lattice vector *a* of the unit cell.

In conclusion, the chirality of the domains can be easily explained by the underlying molecular arrangement, i.e., the oblique subcell. The molecular chirality is reflected in the outer shape of the supramolecular aggregates. Furthermore, the unusual observation that the branching occurs on one single side of each main strand of the hook only has to be pointed out.

***N*-Hexadecanoyl DL-Alanine/H<sub>2</sub>O.** In Figure 4 the  $\Pi/A$  isotherm ( $T = 298$ ) and a series of BAM images recorded in the course of compression of the racemic *N*-hexadecanoylalanine monolayer are shown. The  $\Pi/A$  isotherm exhibits a characteristic of a less condensed monolayer than the isotherm of the pure L-enantiomer, indicating a preferential homochiral interaction (L:L > D:L). This offers in general the possibility of a chiral phase separation process for the racemate. However, although the BAM images differ substantially from those of the enantiomer, they do not indicate such a separation process. Immediately after reaching the main phase transition of first order (LE  $\rightarrow$  LE/LC), huge domains (up to 10 mm in size) with irregular fractal-like shapes appear (images A–C). Interestingly, their sizes increase only slightly while passing the horizontal plateau of the isotherm, implying that the domains are growing and reach their final size extremely fast. It could be shown by generation of artificial air turbulences over the surface that the single dendritic branches of the domains are not rigid but plastically deformable. The same conclusion can be drawn from images D and E, which show that the domains partly fused with progressive compression. An analysis of the Hausdorff dimension of image A gives a value of 1.78, which deviates only slightly from the theoretical value for two-dimensional DLA growth phenomena of 1.71. The experiments carried out at higher temperatures (303 K) give similar results, except that

the domains were a little smaller (data not shown). It is worth noting that the observed domains that appear just after the beginning of the main phase transition did not change their shape significantly for at least 1 h under relaxation conditions (data not shown).

Due to the absence of enantiomer-specific or chiral domain shapes and the nonequilibrium conditions of their growth, the occurrence of a chiral phase separation process does not seem likely. Instead, the presence of true racemic aggregates is more probable, which would imply stronger heterochiral interactions. However, this is in contrast to the thermodynamic (macroscopic scale) behavior as deduced from the  $\Pi/A$  isotherms as well as to the infrared reflection–absorption measurements (molecular scale), where higher conformational order of the alkyl chains of the enantiomeric monolayer was observed.<sup>42</sup> The seemingly contradictory results obtained for different scales suggest that the underlying enantioselective interactions have different relative weights in different kinds of experiments and their strength can vary on different length scales. It is not unusual to detect different chiral preferences with different methods. Furthermore, regarding the probability of a chiral separation process, the fast growth of the domains and the details of the DLA mechanism have to be considered: Assuming relatively strong interactions between the amphiphiles, disregarding their chirality, a particle once adsorbed at the fast growing domain boundary will be permanently associated without the possibility to escape or to change position within the domain. However, at least a minimum of lateral diffusion ability would be a crucial condition for forming separated enantiomeric domains out of the racemate during the course of the condensation. A general hypothesis can be concluded from these observations regarding the principle prerequisite for a chiral phase separation process: The interactions between the enantiomers of opposite handedness have to be weaker than those between enantiomers of the same configuration, where the interaction energy differences may depend on the specific structures. However, the kinetic parameters play an important role as well in determining the structure of the observed domains, because sufficiently strong D:L interactions, though weaker than D:D and L:L interactions, may spontaneously lead to DL domains, the formation of which may retard a chiral phase separation considerably. If the growing velocity of the latter domains is high and only a few domains will be formed, which tend to remain in their initially built state due to the extreme slow relaxation behavior, the probability for observing evidence of a chiral symmetry breaking process that may be intrinsic to the system is low. Vice versa, if the nucleation velocity is high (forming high numbers of nucleation centers per time unit) and the velocity of growth is low, the condition for observing manifestations of a chiral phase separation in the domain structures should be favorable.



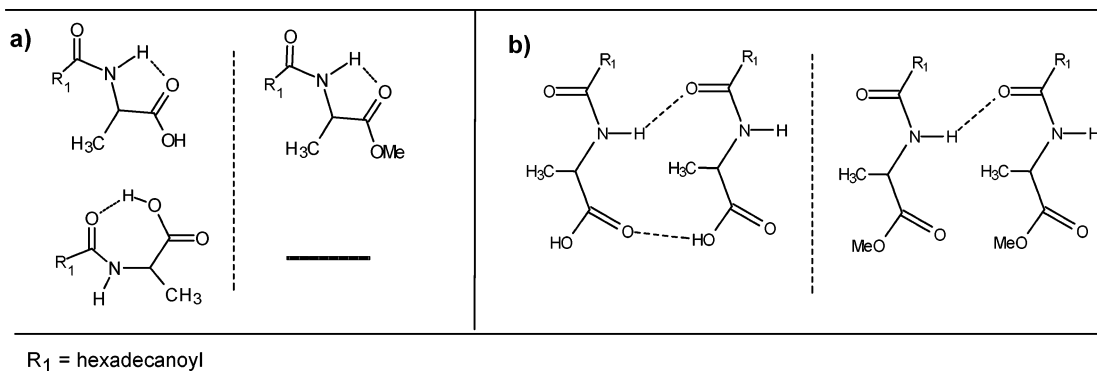


**Figure 7.** Representation of the possibilities to form (a) intra- and (b) intermolecular H-bonds in monolayers of *N*-hexadecanoyl alanine (on the left side of the dotted line) and *N*-hexadecanoyl alanine methyl ester (on the right side of the dotted line).

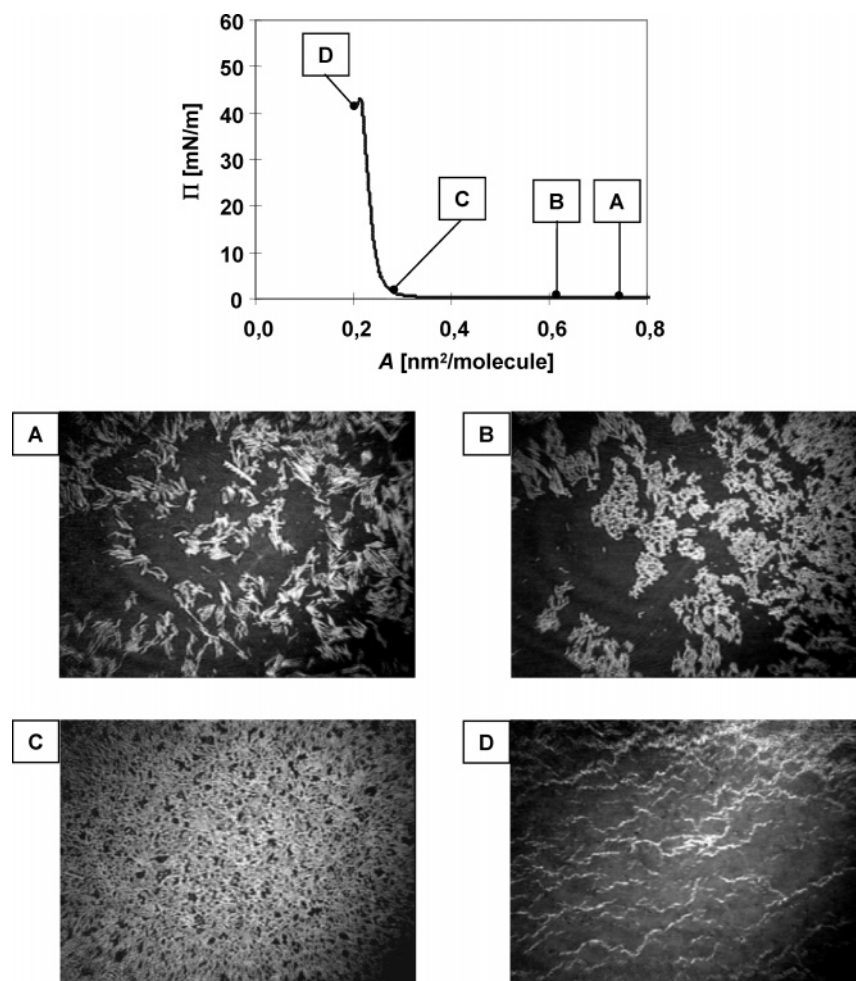


**Figure 8.**  $\Pi/A$  isotherm and corresponding BAM images (A–D) of *N*-hexadecanoyl L-alanine methyl ester on a pure aqueous subphase (pH 6,  $T = 298$  K). The images were recorded at the points indicated on the  $\Pi/A$  plot. They represent an area of  $W \times H = 6 \times 4$  mm.

***N*-Hexadecanoyl L-Alanine/ $\text{Zn}^{2+}$ .** In Figure 5, the  $\Pi/A$  isotherm ( $T = 298$  K) and a series of BAM images of the *N*-hexadecanoyl L-alanine monolayer on a zinc cation containing subphase are presented. The isotherm reflects a monolayer that in comparison to the monolayer on the pure aqueous subphase exhibits a considerably more expanded character, which implies that the surface pressure at a given area/molecule value is higher and that the area/molecule value at a given surface pressure is larger. This shows the typical phenomenon of an overshoot: i.e., the phase transition point ( $0.35 \text{ nm}^2/\text{molecule}/9.5 \text{ mN/m}$ ) lies at higher values than the mean value of the “plateau” region, which in fact deviates from a strictly horizontal course. Immediately after reaching the inflection point, condensed

domains of notable and remarkable shapes appear (image A). Among torus-like domains strongly wound S-shaped structures are visible. They are two-dimensionally chiral, and all of them have the same rotational sense; the corresponding mirror images (question mark shapes) could not be observed. Several repetitions of the BAM experiment revealed that (i) permanently new domains were formed almost during the complete condensation course (in contrast to the processes at 303 K on the pure aqueous subphase) and (ii) the domains show at least two interesting metamorphosis processes. In image B three stages of domain shapes can be observed representing different growth developments: ①, torus-like shapes; ②, S-shaped structures; and ③, domains of seahorse-like appearance. In later states of compres-

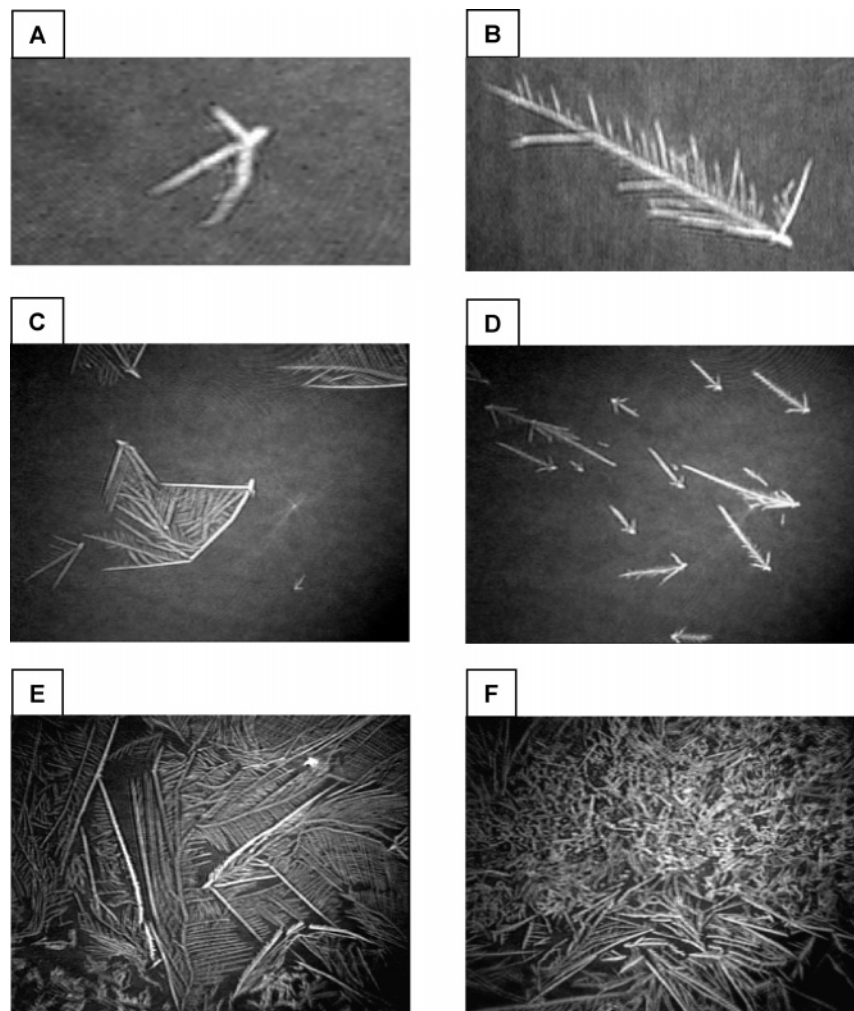


**Figure 9.** Selective BAM images recorded during the spreading procedure of *N*-hexadecanoyl L-alanine methyl ester on a pure aqueous subphase (pH 6,  $T = 298$  K). The size of the spreading droplets was varied in the order image A < image C < image E, and the dipping frequency was varied in the order image B < image D. The pattern observable in image F evolved approximately 2 min after the spreading procedure was finished. Images A and B represent an area of  $W \times H = 2 \times 0.8$  mm; images C–F represent an area of  $W \times H = 6 \times 4$  mm.

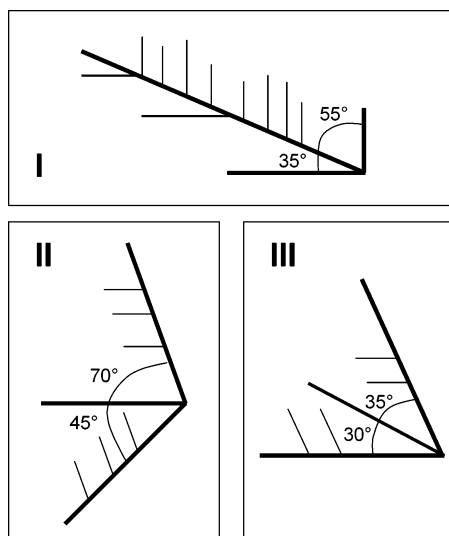


**Figure 10.** Schematic geometric representation of the three different domain types (I–III), observed during the spreading procedure of monolayers of *N*-hexadecanoyl L-alanine methyl ester.

sion they aggregate to extended clusters (image C) and the number of spots with very high brightness is increasing, indicating partial microscopic collapse processes (building of three-dimensional crystallites), before the macroscopic collapse

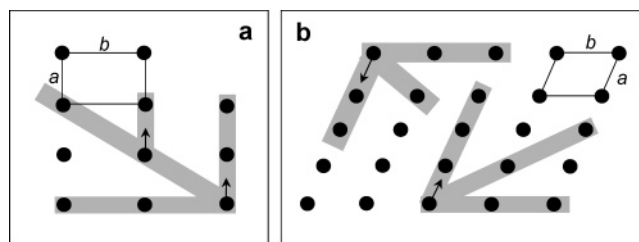


**Figure 11.** Proposed model of correlation between crystal structures and domain shapes, observed during the spreading procedure of *N*-hexadecanoyl L-alanine methyl ester. (a) Domain type I; (b) domain types II and III (see Figure 10). The positions of the amphiphiles are indicated as filled circles; the gray lines represent the main growth directions. The arrows show the possible direction of the azimuthal tilt. In the top left and top right corners, respectively, the subcells are drawn with the lattice vectors  $a$  and  $b$ .

point is reached (images D and E). Unfortunately, it was not possible to check if the domains are exclusively 2D at the beginning of the main phase transition (image A) or if they show a small expansion in the third dimension. In addition, as stated before, the BAM lacks an analyzer and, therefore, a test on reflectivity inversion could not be carried out.

Obviously, the zinc cations possess the ability to influence the aggregation behavior of the amphiphiles in such a way that chiral domains—at least as intermediates—were induced. The



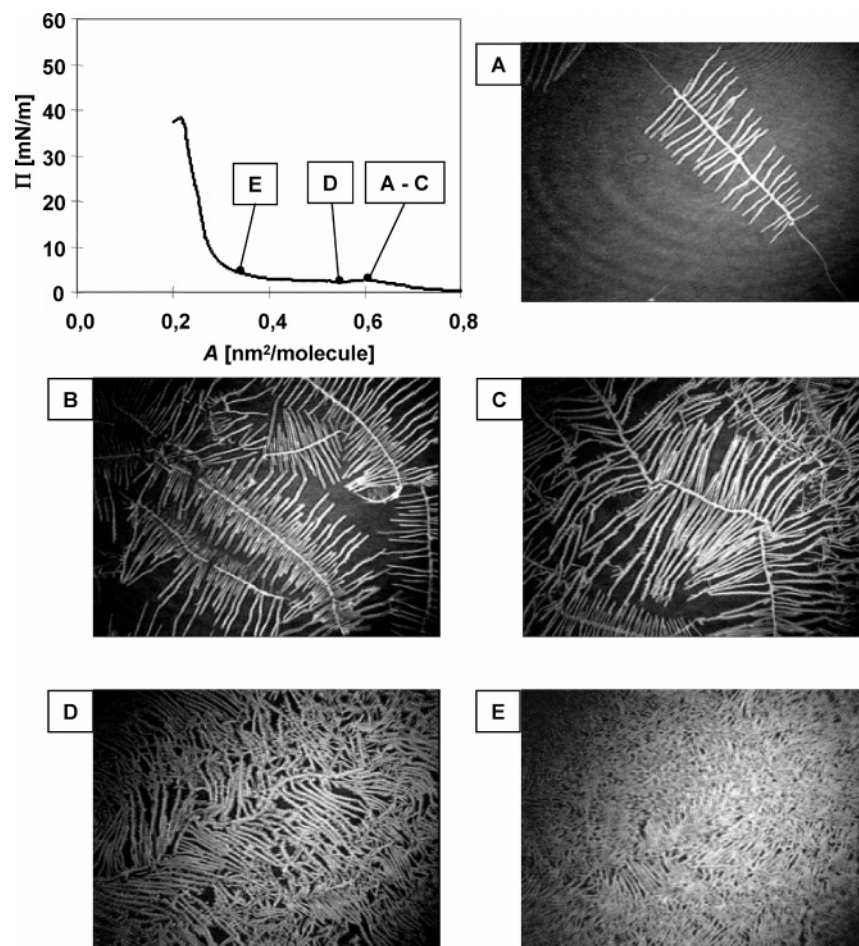


**Figure 12.**  $\Pi/A$  isotherm and corresponding BAM images (A–E) of *N*-hexadecanoyl DL-alanine methyl ester on a pure aqueous subphase (pH 6,  $T = 298$  K). The images were recorded at the points indicated on the  $\Pi/A$  plot. They represent an area of  $W \times H = 6 \times 4$  mm.

formation of chiral domain shapes can be explained by the theoretical concept of asymmetric line tension of domain boundaries, introduced by the pioneering work of McConnell.<sup>63</sup> This concept was originally developed for liquid domains. Here, rigid, crystalline-like domains are present. Therefore, formation of chiral shapes is assumed to be related to inherent chiral growth processes. The prerequisite for such a process in monolayers is an *in-plane* dipole moment (parallel to the interface). Then even achiral molecules can build chiral aggregates by an electrostatically driven growth mechanism, as shown by Sandler et al.<sup>64</sup> However, in this case, left- and right-handed shapes are randomly built. Shapes of one handedness can be expected only if the particles are chiral themselves and are of the same configuration (of the same “sign”). Interestingly, Sandler et al.<sup>65</sup> showed by a Monte Carlo scheme that in fact S-shaped and seahorse-like shapes were preferred.

Consideration of an *in-plane* dipole moment in the present case has to take into account two facts: First, several X-ray diffraction studies have shown that *N*-acyl amino acid derivatives at the air/water interface have tilt angles of at least  $27^\circ$ ,<sup>48,66</sup> because of their relatively large headgroups. Second, the amphiphiles undergo complexation with the zinc cations. Disregarding the true nature of the bond, which is not completely solved yet,<sup>42</sup> it is clear that the projection of the dipole vector onto the *xy*-plane (parallel to the interface) gives a component with a value different from zero. Therefore, it is plausible that the electrostatic growth mechanism is responsible for the pattern observed. To the authors’ knowledge no similar case—the generation of chiral domains of Langmuir monolayers by metal complex formation—has been described in the literature before.

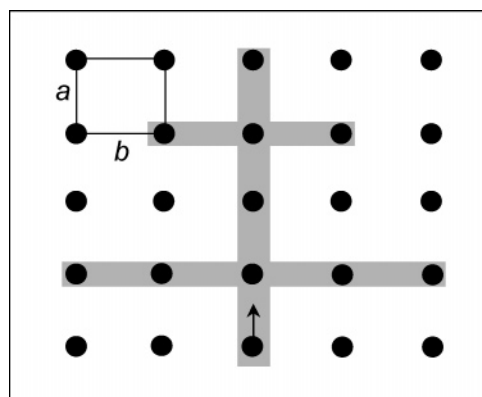


**Figure 13.** Proposed model of correlation between crystal structures and domain shapes of monolayers of *N*-hexadecanoyl DL-alanine methyl ester. The positions of the amphiphiles are indicated as filled circles; the gray lines represent the main growth directions. The arrow shows the possible direction of the azimuthal tilt. In the top left corner the rectangular subcell is drawn with the lattice vectors *a* and *b*.

***N*-Hexadecanoyl DL-Alanine/ $\text{Zn}^{2+}$ .** The  $\Pi/A$  isotherm (298 K) of the racemate of *N*-hexadecanoyl alanine on zinc cation containing subphases is shown in Figure 6. Since it exhibits a more expanded characteristic than the isotherm of the pure enantiomer—as reflected by the considerably higher surface pressure during the course of the compression—homochiral preferences can be noticed. This result implies that the general condition of a potential chiral phase separation process is fulfilled (homochiral preference means a stronger L:L than D:L

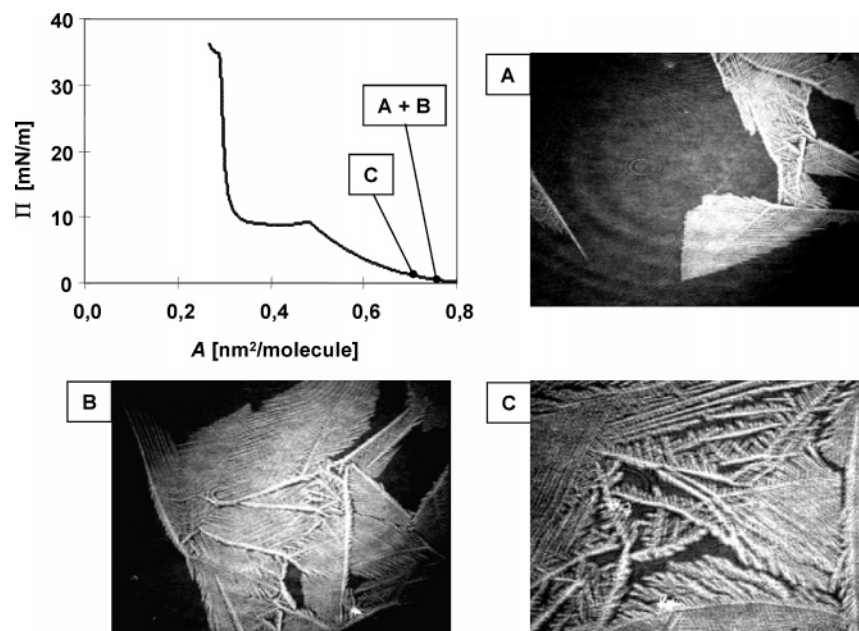


**Figure 14.**  $\Pi/A$  isotherm and corresponding BAM images (A–C) of *N*-octadecanoyl L-valine on a pure aqueous subphase (pH 2,  $T = 298$  K). The images were recorded at the points indicated on the  $\Pi/A$  plot. They represent an area of  $W \times H = 6 \times 4$  mm.

interaction and is a prerequisite for the process of demixing of the enantiomers). However, the zinc ions have such an expanding effect on the monolayer that no main phase transition at all along the whole course of compression occurred. Only just before the collapse point some small condensed domains are observable (Figure 6, image A). Their high reflectivity indicates that they are three-dimensional crystalline nuclei. Furthermore, with high digital magnification some grit-like grainy textures can be seen, but there are no hints that chiral shaped domains were formed. The thermodynamic behavior remained almost unchanged down to 286 K (13 °C), and the same holds for the textures observed with the BAM. It should be noted that the resolution of the BAM is limited to 20  $\mu\text{m}$ ; therefore, it could not be ruled out that chiral symmetry breaking processes took place on length scales smaller than 20  $\mu\text{m}$ . However, it is very unlikely due to the absence of a main phase transition.

***N*-Hexadecanoylalanine Methyl Ester.** The esterification of the carbon acid group of the headgroup restricts the possibilities of forming intra- and intermolecular H-bonds (see Figure 7), raising the question of to what extent the ability to form stable 2D networks of amphiphiles is affected and which consequences result with regard to the chiral preference and domain shapes. Again, the pure enantiomeric monolayer (L) is compared with the racemic mixture (DL).

**L-Monolayer.** The  $\Pi/A$  isotherm ( $T = 298$  K) of the pure L-monolayer and a series of BAM images are presented in Figure 8. The isotherm shows the same condensed characteristic as the corresponding monolayer of the free acid amphiphile, and crystal-like structures were also observed immediately after the spreading procedure (image A). However, in contrast to the free acid, the domains of the methyl ester are much smaller, considerably less compact, and far more numerous. Images B and C give indications that the domains are fragile, and the cohesive forces between the amphiphiles seem to be much smaller than in the case of the free acid. A plausible explanation is that one of the possibilities to form hydrogen bonds is missing. Interestingly, the less pronounced cohesion between the amphiphiles finds its IR spectroscopic expression in the circumstance that, in the early course of compression in comparison to the free acid, higher wavenumbers of the antisymmetric C–H-

stretch vibrations were measured as found in a complementary study where the order of the domains on a molecular scale was the focus.<sup>42</sup> These higher wavenumbers indicate that the packing density is less and the number of *gauche* defects (synclinal conformations) of the alkyl chains is higher.

Inspired by the brittle nature of the domains and the fact that high fractions of the area were covered with film material after the spreading procedure, we had speculated that the domains shown in image A were not in a “virgin” state, i.e., that they already have undergone a transformation process. Accordingly, we carried out several experiments with variable amounts of spreading volume (at constant spreading solution concentrations) as well as with variation in the dropping frequency of the spreading syringe. The resulting BAM images are shown in Figure 9. Three different types (I–III) of dendritic domains were predominant, which are schematically sketched in Figure 10, where the main geometric features are given. Domain type I can be derived from a rectangular subcell, whereas both types II and III can be constructed on the same single oblique subcell (see Figure 11). The fact that more than one specific dendritic pattern is present at the same time is rare. However, Vollhardt et al.<sup>30</sup> showed that the angle and number of the branches of dendritic domains can vary with the local growth rate, and therefore even the underlying lattice type can be different. Studying the evolution of the dendrites in terms of time was not possible because this process was by far too fast: the domains grew in fractions of a second. It is also important to bear in mind that these structures are only visible at the very beginning of the spreading procedure, indicating that they are nonequilibrium structures and that it is, therefore, very likely that these structural features are only temporary and will change with time.

**DL-Monolayer.** The  $\Pi/A$  isotherm ( $T = 298$  K) and the corresponding morphological features of the racemic mixture of *N*-hexadecanoyl alanine methyl ester are shown in Figure 12. With the beginning of the main phase transition, condensed structures of large but filigree dendritic-like shape appear (image A). They are characterized by a linear main strand and almost parallel and equidistant branches in the perpendicular direction. With ongoing compression the length of both the main strand

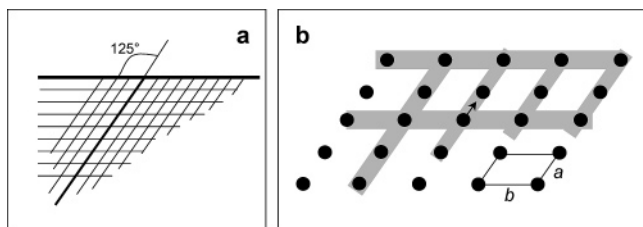


**Figure 15.** (a) Schematic geometric representation of the domains of *N*-octadecanoyl L-valine. (b) Proposed model of correlation between the crystal structure and the domain shape. The positions of the amphiphiles are indicated as filled circles; the gray lines represent the main growth directions. The arrow shows the possible direction of the azimuthal tilt. In the bottom right corner the oblique subcell is drawn with the lattice vectors *a* and *b*.

and branches as well as the number of branches increases (image B). The growth of the thickness plays a minor role in comparison to the growth of the length. The branches of the domains are deformable and not fragile, they do not break apart by collision (see image C), and they seem to be less brittle than the domains formed by the pure enantiomeric monolayer.

Again, it is possible to construct an underlying lattice type that could explain the observed domain shapes. The two distinctive main growth directions can be derived on the basis on a rectangular subcell (see Figure 13).

Regarding the question of whether a chiral phase separation takes place or not, the thermodynamic (compare the isotherms) and IR spectroscopic data<sup>42</sup> give evidence that it is possible. The cited IRRAS study indicates that the enantiomeric and racemic monolayers—despite their different morphologies and subcell types—achieve comparable packing densities. However, the recorded BAM images do not give any hint that a segregation process occurred which would lead to enantiomeric domains of opposite handedness.

***N*-Octadecanoylvaline.** In order to study the influence of alkyl chain lengths, of the headgroup sizes, and of polarity on the film morphology and particularly on potential chiral discrimination effects, monolayers of *N*-octadecanoyl valine were investigated. Parazak et al.,<sup>29</sup> who studied the racemic monolayer with fluorescence microscopy, observed left- and

right-handed curved domains. On the other hand, IRRA spectroscopic measurements revealed only weak homochiral discrimination effects.<sup>42</sup>

**L-Monolayer.** In Figure 14 the  $\Pi/A$  isotherm (pH 2,  $T = 298$  K) and a series of BAM images of the L-monolayer are presented. Already during the early stage of compression, which may be assigned to a LE phase, extended dendritic structures appear, resembling feathers (images A and B). The branching density is extraordinarily high, and almost closed compact structures appear. The dendritic morphology is only visible at higher magnification, particularly at the boundaries of the domains (see image C), which partially overlap. However, because of the different overall appearance of image C, it is not possible to rule out another phase transition (of unknown nature) at this point, even though it is not detectable in the isotherm. The main geometric features and the possible oblique underlying subcell of the dendritic domains are shown in Figure 15.

Due to the uncommon and conspicuous thermodynamic behavior, i.e., the occurrence of condensed structures before the plateau of the isotherm is reached, further investigations regarding the reversibility of the domain formation were carried out. After the collapse of the monolayer, reexpansion and subsequent second compression were carried out. The expansion isotherm and representative BAM images are shown in Figure 16. At the beginning of the expansion the surface pressure sharply decreases until a plateau is reached, the surface pressure level of which (8.8 mN/m) lies only slightly below that of the compression course (9.4 mN/m); i.e., the hysteresis effect is comparably small. Further increase in area per molecule causes the domains to break apart (image A), followed by melting or spreading processes, respectively (image B). At 0.8 nm<sup>2</sup>/molecule the whole film-covered area is free of condensed structures. Compressing the monolayer again, at only slightly higher surface pressures the building of dendritic domains was observable again (image C).

In summary, the following conclusions can be drawn. (i) Like the L-enantiomers of *N*-hexadecanoyl alanine and its methyl ester, the monolayers of *N*-octadecanoyl L-valine form crystalline dendritic domains; however, they differ in several aspects:

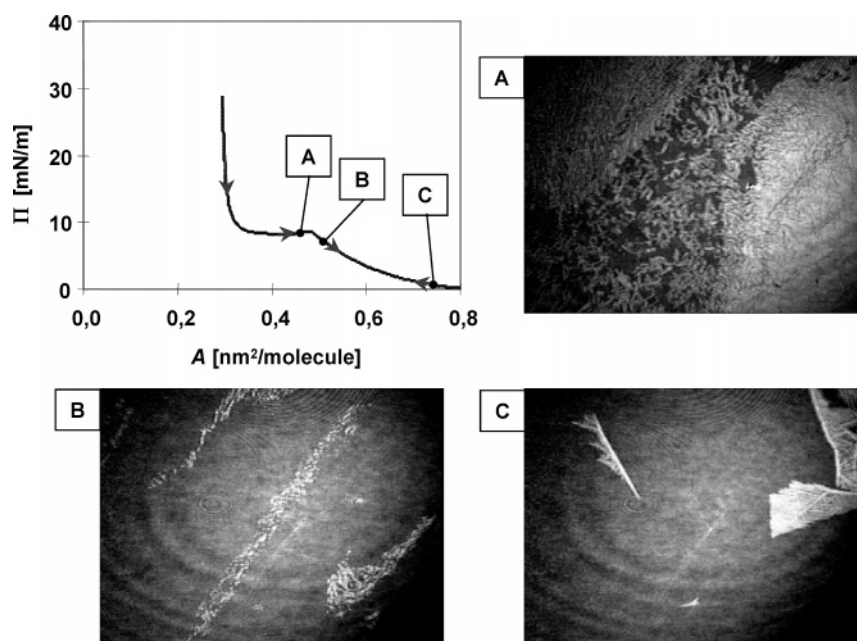


**Figure 16.** BAM images of *N*-octadecanoyl L-valine on a pure aqueous subphase (pH 2,  $T = 298$  K) recorded at the points indicated on the  $\Pi/A$  plot during the expansion cycle (A and B) and recompression cycle (C). They represent an area of  $W \times H = 6 \times 4$  mm.



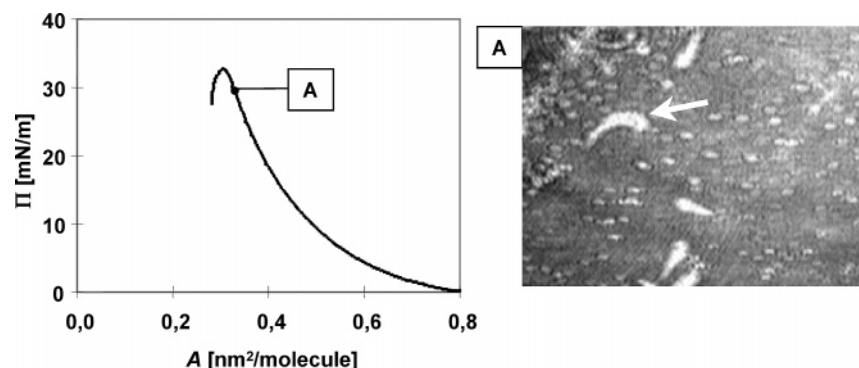


**Figure 17.**  $\Pi/A$  isotherm and one corresponding BAM image of *N*-octadecanoyl DL-valine on a pure aqueous subphase (pH 2,  $T = 298$  K) recorded at the point indicated on the  $\Pi/A$  plot. It represents an area of  $W \times H = 2.9 \times 2$  mm. The features of the domain marked with an arrow are explained in the text.

the branching density is substantially higher, the individual dendrites are noticeably thinner, and the texture is more uniform and regular. (ii) The emergence of the crystalline dendritic domains is fully reversible, in contrast to the other substances investigated. The growth of the domains takes place at lower rates and closer to the thermodynamic equilibrium. This could be an explanation for the regularity of the dendrites of the domains. (iii) In the complementary IRRAS study at high area per molecule values a relatively low degree of conformational order of the acyl chains was detected. This means that a high long-range positional order of the headgroups is sufficient to build regular crystal-like structures, or inversely, due to the relatively voluminous valine headgroup, the conformational order of the acyl chains is not automatically high, even when the amphiphiles are in a crystal-like arrangement.

**DL-Monolayer.** The  $\Pi/A$  isotherm (pH 2,  $T = 298$  K) and one representative BAM image of the racemic monolayer of *N*-octadecanoyl valine, recorded just before the collapse point, are shown in Figure 17. Among many small domains of unspecific shapes a few bigger domains ( $\sim 200 \mu\text{m}$ ) were visible, which have a rounded head and a longer tail; in some cases the tails were curved (marked with an arrow in image A). Whether the number of tails are randomly partitioned into right- and left-handed ones could not be ascertained, because they were generally too small to determine the rotating sense unequivocally.

The observations of Parazak et al.<sup>29</sup> could not be confirmed, and we think it is generally very unlikely that chiral phase separation processes occur in cases where no main phase transition is present. However, it cannot be excluded that the resolution of the BAM is insufficient.

## Conclusions

Investigations on the aggregation behavior and morphology of Langmuir films of enantiomeric (L) and racemic (DL) *N*-acyl amino acids on pure aqueous as well metal cation containing subphases carried out at the mesoscale level with the help of Brewster angle microscopy (BAM) supplied the results as follows:

(i) The L-enantiomer of *N*-hexadecanoyl alanine on a pure aqueous subphase at 298 K forms crystal platelets, while the growth mechanism in the case of the racemic mixture leads to irregular fractal-like domain shapes, implying a field, which follows a Laplacian equation with a proper boundary condition. At 303 K the L-enantiomer shows a dendritic growth pattern, which leads to explicitly chiral domain shapes for which hydrogen bridges as directed attractive forces are assumed to be responsible.

(ii) Compression of the L-enantiomer on a zinc ion containing subphase is accompanied by a remarkable metamorphosis of the condensed structure. Starting from torus-like domains, they were at first converted into strongly wound S-shaped domains, finally turning into a seahorse-like appearance. The origin of these chiral shapes can be explained on the basis of an electrostatic growth model.

(iii) The enantiomer of *N*-hexadecanoyl alanine methyl ester shows three different asymmetric dendritic growth patterns. The domains of the racemic mixture are dendritic too, but in contrast they are symmetric and have a notably low branching density.

(iv) On a pure aqueous subphase the L-enantiomer of *N*-octadecanoyl valine exhibits dendritic growth as well, but the overall outer shape of the domains is not explicitly chiral.

**Acknowledgment.** This work was supported by the Fonds der Chemischen Industrie, Germany. F.H. thanks Ninja Reineke for revising the manuscript.

## References and Notes

- (1) Podlech, J. *Cell. Mol. Life Sci.* **2001**, 58, 44.
- (2) Cronin, J. R.; Pizzarello, S. *Science* **1997**, 275, 951.
- (3) Green, M. M.; Selinger, J. V. *Science* **1998**, 282, 880.
- (4) Kondepudi, D. K. *Biosystems* **1987**, 20, 75.
- (5) Kondepudi, D. K.; Kaufman, R. J.; Singh, N. *Science* **1990**, 250, 975.
- (6) Kondepudi, D. K.; Laudadio, J.; Asakura, K. *J. Am. Chem. Soc.* **1999**, 121, 1448.
- (7) Szabó-Nagy, A.; Keszthelyi, L. *Proc. Natl. Acad. Sci. U.S.A.* **1999**, 96, 4255.
- (8) Soai, K.; Shibata, T.; Morioka, H.; Choji, K. *Nature* **1995**, 378, 767.
- (9) Shibata, T.; Morioka, H.; Hayase, T.; Choji, K.; Soai, K. *J. Am. Chem. Soc.* **1996**, 118, 471.
- (10) Kitamura, M.; Suga, S.; Oka, H.; Noyori, R. *J. Am. Chem. Soc.* **1998**, 120, 9800.
- (11) Zepik, H.; Shavit, E.; Tang, M.; Jensen, T. R.; Kjaer, K.; Bolbach, G.; Leiserowitz, L.; Weissbuch, I.; Lahav, M. *Science* **2002**, 295, 1266.
- (12) Selinger, J. V.; Wang, Z.-G.; Bruinsma, R. F.; Knobler, C. M. *Phys. Rev. Lett.* **1993**, 70, 1139.
- (13) Xu, J.; Selinger, R. L. B.; Selinger, J. V.; Shashidhar, R. *J. Chem. Phys.* **2001**, 115, 4333.
- (14) Weissbuch, I.; Addadi, L.; Berkovitch-Yellin, Z.; Gati, E.; Lahav, M.; Leiserowitz, L. *Nature* **1984**, 310, 161.
- (15) Lösche, M.; Sackmann, E.; Möhwald, H. *Ber. Bunsen-Ges. Phys. Chem.* **1983**, 87, 848.
- (16) Weiss, R. M.; McConnell, H. M. *Nature* **1984**, 310, 47.
- (17) Rietz, R.; Brezesinski, G.; Möhwald, H. *Ber. Bunsen-Ges. Phys. Chem.* **1993**, 97, 1394.
- (18) Nassoy, P.; Goldmann, M.; Bouloussa, O.; Rondelez, F. *Phys. Rev. Lett.* **1995**, 75, 457.
- (19) Rietz, R.; Rettig, W.; Brezesinski, G.; Bouwman, W. G.; Kjaer, K.; Möhwald, H. *Thin Solid Films* **1996**, 284/285, 211.
- (20) Sandler, I. M.; Canright, G. S.; Zhang, Z.; Gao, H.; Xue, Z.; Pang, S. *Phys. Lett. A* **1998**, 245, 233.

- (21) Stine, K. J. In *Encyclopedia of Surface and Colloid Science*; Hubbard, A. T., Ed.; Marcel Dekker: New York, 2002; p 1017.
- (22) Harvey, N. G.; Rose, P. L.; Mirajovsky, D.; Arnett, E. M. *J. Am. Chem. Soc.* **1990**, *112*, 3547.
- (23) Heath, J. G.; Arnett, E. M. *J. Am. Chem. Soc.* **1992**, *114*, 4501.
- (24) Akamatsu, S.; Bouloussa, O.; To, K.; Rondelez, F. *Phys. Rev. A* **1992**, *46*, 4504.
- (25) Weissbuch, I.; Leveiller, F.; Jacquemain, D.; Kjaer, K.; Als-Nielsen, J.; Leiserowitz, L. *J. Phys. Chem.* **1993**, *97*, 12858.
- (26) Stine, K. J.; Uang, J. Y.-J.; Dingman, S. D. *Langmuir* **1993**, *9*, 2112.
- (27) Gericke, A.; Hühnerfuss, H. *Langmuir* **1994**, *10*, 3782.
- (28) Stine, K. J.; Whitt, S. A.; Uang, J. Y.-J. *Chem. Phys. Lipids* **1994**, *69*, 41.
- (29) Parazak, D. P.; Uang, J. Y.-J.; Turner, B.; Stine, K. J. *Langmuir* **1994**, *10*, 3787.
- (30) Vollhardt, D.; Gutberlet, T.; Emrich, G.; Fuhrhop, J. H. *Langmuir* **1995**, *11*, 2661.
- (31) Parazak, D. P.; Uang, J. Y.-J.; Whitt, S. A.; Stine, K. J. *Chem. Phys. Lipids* **1995**, *75*, 155.
- (32) Uang, J. Y.-J.; Parazak, D. P.; Stine, K. J. *Chem. Phys. Lipids* **1995**, *75*, 163.
- (33) Stine, K. J.; Leventhal, A. R.; Parazak, D. P.; Uang, J. Y.-J. *Enantiomer* **1996**, *1*, 41.
- (34) Hühnerfuss, H.; Neumann, V.; Stine, K. J. *Langmuir* **1996**, *12*, 2561.
- (35) Hühnerfuss, H.; Gericke, A.; Neumann, V.; Stine, K. J. *Thin Solid Films* **1996**, *284/285*, 694.
- (36) Rudert, R.; André, Ch.; Wagner, R.; Vollhardt, D. *Z. Kristallogr.* **1997**, *212*, 752.
- (37) Melzer, V.; Weidemann, G.; Vollhardt, D.; Brezesinski, G.; Wagner, R.; Struth, B.; Möhwald, H. *Supramol. Sci.* **1997**, *4*, 391.
- (38) Melzer, V.; Weidemann, G.; Vollhardt, D.; Brezesinski, G.; Wagner, R.; Struth, B.; Möhwald, H. *J. Phys. Chem. B* **1997**, *101*, 4752.
- (39) Weissbuch, I.; Berfeld, M.; Bouwman, W.; Kjaer, K.; Als-Nielsen, J.; Lahav, M.; Leiserowitz, L. *J. Am. Chem. Soc.* **1997**, *119*, 933.
- (40) Rietz, R.; Rettig, W.; Brezesinski, G.; Möhwald, H. *Pharmazie* **1997**, *52*, 701.
- (41) Du, X.; Shi, B.; Liang, Y. *Langmuir* **1998**, *14*, 3631.
- (42) Hoffmann, F.; Hühnerfuss, H.; Stine, K. J. *Langmuir* **1998**, *14*, 4525.
- (43) Du, X.; Liang, Y. *J. Phys. Chem. B* **2000**, *104*, 10047.
- (44) Zhang, Y. J.; Song, Y.; Zhao, Y.; Li, T. J.; Jiang, L.; Zhu, D. *Langmuir* **2001**, *17*, 1317.
- (45) Mao, L.; Harris, H. H.; Stine, K. J. *J. Chem. Inf. Comput. Sci.* **2002**, *42*, 1179.
- (46) Andelman, D. *J. Am. Chem. Soc.* **1989**, *111*, 6536.
- (47) Andelmann, D.; Orland, H. *J. Am. Chem. Soc.* **1993**, *115*, 12322.
- (48) Nandi, N.; Vollhardt, D. *Colloids Surf., A: Physicochem. Eng. Aspects* **2001**, *183–185*, 67.
- (49) Nandi, N.; Vollhardt, D. *Colloids Surf., A: Physicochem. Eng. Aspects* **2002**, *198–200*, 207.
- (50) Nandi, N.; Vollhardt, D. *J. Phys. Chem. B* **2003**, *107*, 3464.
- (51) Suresh, K. A.; Nittmann, J.; Rondelez, F. *Europhys. Lett.* **1988**, *6*, 437.
- (52) Weidemann, G.; Vollhardt, D. *Biophys. J.* **1996**, *70*, 2758.
- (53) Weidemann, G.; Vollhardt, D. *Colloids Surf., A* **1995**, *100*, 187.
- (54) Adam, J.; Rettig, W.; Duran, R. S.; Naciri, J.; Shashidhar, R. *J. Phys. Chem.* **1993**, *97*, 2021.
- (55) Miyano, K.; Tamada, K. *Langmuir* **1993**, *9*, 508.
- (56) Witten, T. A.; Sander, L. M. *Phys. Rev. Lett.* **1981**, *47*, 1400.
- (57) Witten, T. A.; Sander, L. M. *Phys. Rev. B* **1983**, *27*, 5686.
- (58) Bruinsma, R.; Rondelez, F.; Levine, A. *Eur. Phys. J. E* **2001**, *6*, 191.
- (59) Brener, E.; Müller-Krumbhaar, H.; Temkin, D.; Abel, T. *Physica A* **1998**, *249*, 73.
- (60) Lauher, J. W.; Chang, Y.-L.; Fowler, F. W. *Mol. Cryst. Liq. Cryst.* **1992**, *211*, 99.
- (61) Gehlert, U.; Weidemann, G.; Vollhardt, D.; Brezesinski, G.; Wagner, R.; Möhwald, H. *Langmuir* **1998**, *14*, 2112.
- (62) Weinbach, S. P.; Jacquemain, D.; Leveiller, F.; Kjaer, K.; Als-Nielsen, J.; Leiserowitz, L. *J. Am. Chem. Soc.* **1993**, *115*, 11110.
- (63) McConnell, H. M.; Moy, V. T. *J. Phys. Chem.* **1988**, *92*, 4520.
- (64) Sandler, I. M.; Canright, G. S.; Zhang, Z.; Gao, H.; Xue, Z.; Pang, S. *Phys. Lett. A* **1998**, *245*, 233.
- (65) Sandler, I. M.; Canright, G. S.; Gao, H.; Pang, S.; Xue, Z.; Zhang, Z. *Phys. Rev. E* **1998**, *58*, 6015.
- (66) Vollhardt, D.; Retter, U. *Langmuir* **1998**, *14*, 7250.